Efficiency of π−π Tunneling in [2]Rotaxane Molecular Electronic Switches

2 AUTHORS, INCLUDING:

William A. Goddard
California Institute of Technology

1,332 PUBLICATIONS   **68,116** CITATIONS

Efficiency of $\pi-\pi$ Tunneling in [2]Rotaxane Molecular Electronic Switches

Yong-Hoon Kim*,† and William A. Goddard, III‡

*Department of Materials Science and Engineering, University of Seoul, 90 Jeonnong-dong,
Dongdaemun-gu, Seoul, 130-743 Korea, and Materials and Process Simulation Center,
California Institute of Technology, Pasadena, California 91125-7400*

We perform large-scale density functional and matrix Green's function calculations, and study the coherent charge tunneling properties of molecular electronic devices based on the central part of [2]rotaxane molecules. We extract molecular core regions from realistic monolayer configurations with folded molecular structures and sandwich them between Au(111) electrodes to form device models. We show that the electrical switching behavior can be observed within the $\pi-\pi$ stacked serial arrangement of redox-active components in the [2]rotaxane monolayer as with the parallel arrangement in the [2]catenane case. We thus demonstrate the effectiveness of the $\pi-\pi$ electron tunneling and the universality of the switching mechanism based on the energetic movement of frontier orbitals accompanying the conformational switching. In addition, via considering the energetic ordering of highest-occupied molecular orbital (HOMO) and HOMO-1 levels that originated from tetrathiafulvalene and dioxynaphthalene in several ground-state conformation device models, we show that the molecule−electrode configurations critically affect the device functionality.

1. Introduction

A successful combination of advanced chemical synthesis techniques[1] (involving supramolecular chemistry and Langmuir film formation) and solid-state device fabrication methods[2] (such as the e-beam lithography) has recently led to the achievement of recyclable [2]rotaxane and [2]catenane molecular electronic switches.[3−5] The[2]catenane and [2]rotaxane molecules employed in the experiments are composed of an electron-accepting cyclobis-(paraquat-*p*-phenylene) (CBPQT^{4+}) ring that encloses a ring-shaped and linear backbone with two electron-donating stations, tetrathiafulvalene (TTF) and the 1,5-dioxynaphthalene (DNP) [parts a and b of Figure 1]. They have bistable conformations: CBPQT^{4+} encircling the stronger donor TTF as the ground state co-conformation (GSCC) and CBPQT^{4+} encircling the weaker donor DNP as the metastable state co-conformation (MSCC) [Figure 1c]. The reversible electrical switching in the device was proposed[3−5] to result from the mechanical switching of the molecule between the OFF-state GSCC and the ON-state MSCC.

However impressive this achievement was, the molecular origin of the device switching has been questioned[6,7] due to some seemingly contradictory experimental results.[8,9] In fact, the switching origin in the latter experiments was traced to the molecule−electrode interface,[9,10] whereas the switching in the original experiments was shown to originate from the molecules themselves.[3−5,11] Nevertheless, the confusion in the molecular electronics community is not fully resolved,[6,7] and we view that the situation largely results from the lack of microscopic understanding of the device function principles in these elegant yet complex devices.

To resolve such controversies and provide a firm ground of developing molecular electronics based on supramolecules, we

have been theoretically investigating the essential features of the device characteristics. In an initial study, one of us employed a simplified device model based on a single extended rotaxane molecule and emphasized the role of spatial distributions of frontier orbitals for the switching.[12] However, the spatial distribution alone cannot fully explain the device function, as can be seen by the fact that the [2]catenane device that has a similar spatial distribution of redox-active elements with respect to the electrodes within GSCC and MSCC also shows a switching behavior. Thus, employing a more accurate modeling of monolayer formation and electrodes, we considered the catenane device and identified the energetic movement of frontier orbitals as its switching origin.[13] We also demonstrated the robustness of the switching behavior with respect to the thermal fluctuation of molecules and the variation of packing density and electrode types.[14]

As the next stage of the study, here we consider the rotaxane device based on the realistic monolayer conformation. The comparative study of rotaxane and catenane devices is not only essential to determine the universality of the switching mechanism we have identified for the catenane case but also to establish the important relationship between molecular structures and device properties. However, the rotaxane device is a more challenging system to treat than the catenane counterpart, because the conformation of monolayers is more complex and the modeling of molecule−electrode interfaces is less straightforward with the stoppers. Thus, we consider a device model based on simplified rotaxane molecular structures and identify important characteristics of devices and molecule-electrode interfaces. We will show that the rotaxane device functions in a similar manner as the catenane device due to the efficient $\pi-\pi$ tunneling within the molecular core region. We will also show that the nature of molecule−electrode interfaces is an important aspect of device function.

The organization of the paper is as follows. In section 2, we briefly summarize our multiscale computational approach. In

---

* To whom correspondence should be addressed. E-mail: y.h.kim@uos.ac.kr.
† University of Seoul.
‡ California Institute of Technology.
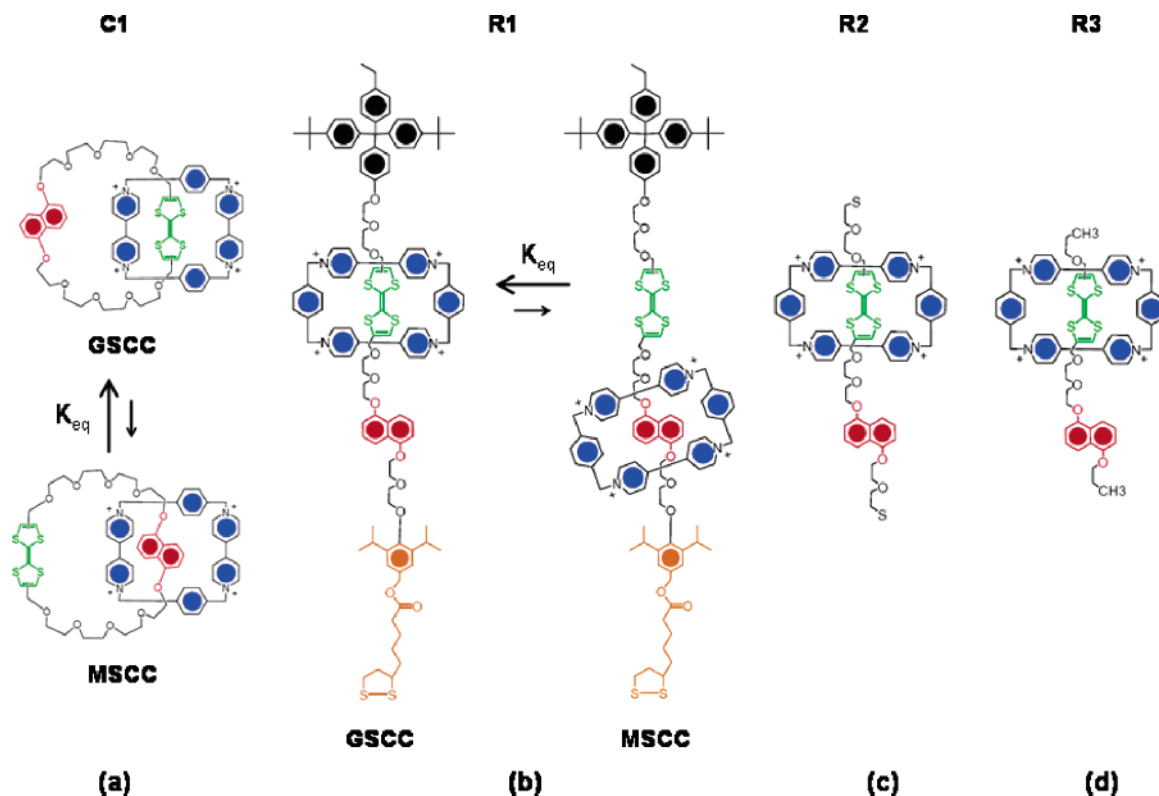
Figure 1. (a) Structural formula of the catenane **C1** (GSCC configuration). (b) Structural formula of the rotaxane **R1** (GSCC configuration) used to study its monolayer formation via force-field MD simulations. (c) Structural formula of the simplified rotaxane (pseudorotaxane) **R2** (GSCC configuration) incorporated between the electrodes for the second-stage molecular dynamics simulations. (d) Structural formula of further simplified pseudorotaxane **R3** incorporated into the device models for the final quantum mechanical DFT and MGF calculations.

section 3.1, we describe how we constructed device models that are simple enough and yet capture the essential features of the molecules in realistic monolayer configurations. In section 3.2, we show that our calculations of coherent charge tunneling properties extract a switching behavior that is similar to that of catenane devices we have previously considered. In section 3.3, by focusing on the energetic ordering of frontier orbitals in GSCC device models, we demonstrate the nontriviality of modeling molecule−metal electrode interface and its importance in determining the device characteristics. Section 4 summarizes the present paper.

2. Computational Details

Our multiscale computational approach consists of the following three stages.

2.1. Force-Field Molecular Dynamics (MD) Simulations for Structural Studies and Statistical Sampling. To obtain realistic conformations of molecules, we first performed force-field MD simulations using the *Cerius2* program (Accelrys). Force-fields were based on the extended generic Dreiding force fields for the nonmetallic atoms[15] extended to describe the Au−Au interactions and the Au−organic nonbond interactions.[16] Employing force fields (which include van der Waals interactions) to obtain molecular structures is necessary not only for numerical efficiency but also because the approximate density functional (section 2.2) does not describe weak van der Waals interactions. Charges were obtained from the charge equilibration model.[17] Details of our MD studies will be presented in section 3.1.

2.2. Density Functional Theory (DFT) Calculations for Electronic Structures. For the device models constructed by sandwiching the molecules between metal electrodes, we next performed DFT calculations using the *SeqQuest* program

(Sandia National Labs) to obtain the Hamiltonian matrices of the device model and corresponding electrodes. We adopted norm-conserving pseudopotentials[18] and a Gaussian basis set of double-ζ-plus-polarization quality for the molecules (H, C, N, F, P, and S) and single-ζ-plus-polarization quality for the electrodes (Au) optimized for the corresponding pseudopotentials. We employed the Perdew−Burke−Enzhrof[19] parametrization of the generalized gradient approximation (GGA). Carrying out a convergence test with respect to the reciprocal-space $\mathbf{k}_{||}$ point sampling along the electrode-surface direction, we found out that, while the highest-occupied molecular orbital (HOMO) and lowest-unoccupied molecular orbital (LUMO) position was reliably estimated via the Γ-point-only sampling, at least a single complex $\mathbf{k}_{||}$-point sampling (shifted off from the Γ point) is required for the accurate estimation of the energetic position of states located at further away from E_F and to produce the numerically negligible gap of device model and corresponding electrodes.[20] We finally comment that the role of van der Waals interactions, which are not properly described by GGA, is limited to the determination of molecular structures. Once the geometries are known, then their electronic properties including charge transport characteristics (section 2.3) should weakly depend on van der Waals interactions, so our GGA results should be valid at the qualitative level. However, because of self-interaction errors in GGA and the resulting band gap underestimation, the location of unoccupied molecular orbitals is expected to be downshifted, and the quantitative accuracy of our study should be limited in that respect (e.g., transmission is expected to be overestimated).

2.3. Matrix Green's Function Calculations for the Device Charge Transport Properties. With the density-functional calculation output, we finally performed the matrix

Efficiency of $\pi-\pi$ Tunneling

J. Phys. Chem. C, Vol. 111, No. 12, 2007 **4833**
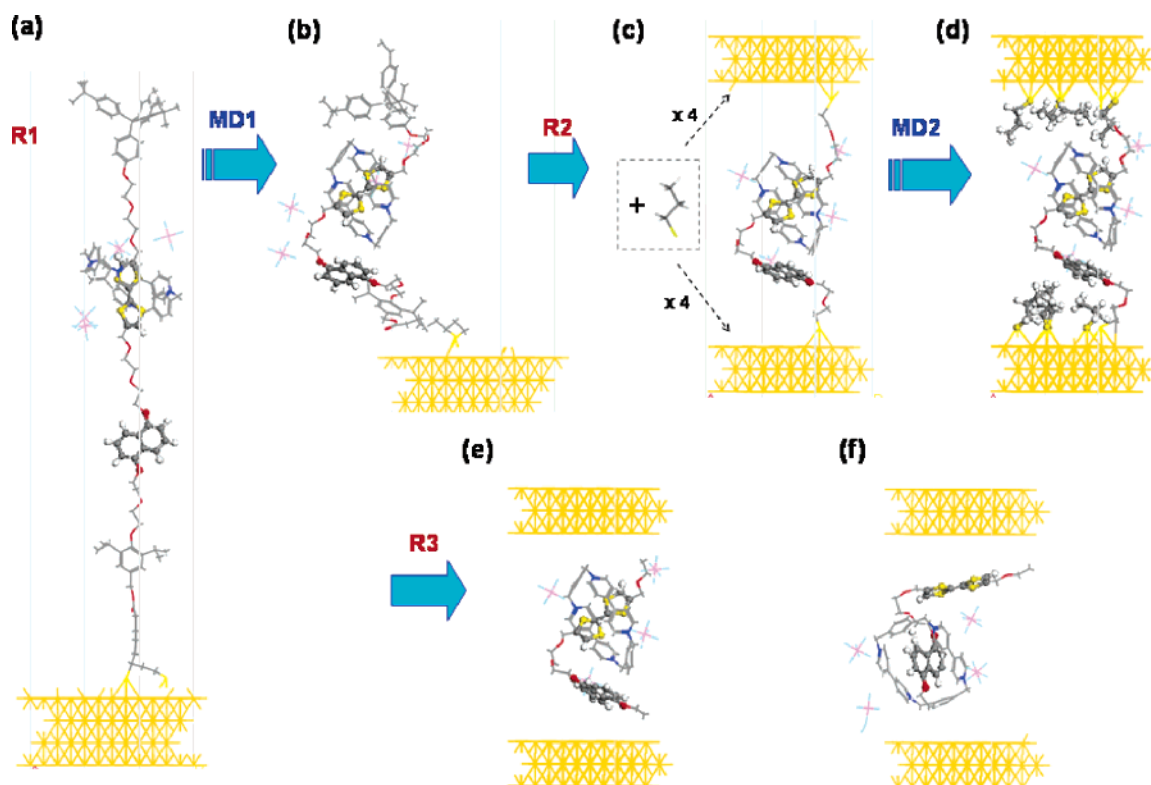
Figure 2. (a–e) Schematic procedure of constructing a GSCC monolayer device model for MGF calculations based on the pseudorotaxane **R3** starting from the full 4 × 4-Au (111)-cell rotaxane **R1** SAM. While the height of the fully stretched molecule (a) is 65 Å, that of the relaxed folded molecule is only 34 Å, which makes the coherent tunneling a relevant charge transport mechanism. The electrode–electrode gap distance of the device based on a simplified molecular structure **R2** (c,d) is 28 Å and that of the device based on a further simplified molecular structure **R3** (e) that preserved only the core of the molecule is 22 Å. (f) Corresponding device model based on MSCC rotaxane **R3**.

Green's function calculation to compute the transmission function[21] where S_M and H_M are, respectively, the molecule parts

$$T(E) = Tr[\Gamma_1(E)G_M(E)\Gamma_2(E)G_M^+(E,V)]$$

$$G_M(E) = (ES_M - H_M - \Sigma_1 - \Sigma_2)^{-1}$$

$$\Sigma_a = x_a g_{Sa} x_a^+$$

$$\Gamma_a = i(\Sigma_a - \Sigma_a^+)(a = 1,2) \qquad (1)$$

of the overlap and Hamiltonian matrices and x_a are the molecule–electrode parts of the total *ES-H* operator. The self-energies Σ provide the ab initio values of the broadening and shift of molecular energy levels resulting from the coupling of molecules to electrodes. The surface Green's functions g_S were extracted from two independent bulk GGA calculations with the unit cells corresponding to the bottom and top electrodes and the single/four $\mathbf{k}_\parallel/\mathbf{k}_\perp$-point sampling along the electrode-surface/normal direction. The energy was first scanned around E_F using 0.01-eV steps, and then the resolution was adaptively increased near the transmission resonance regions up to 0.0001 eV, at which a sufficient level of convergence was reached.

With *T*, the current–voltage (*I*–*V*) characteristics were obtained via the Landauer-type formula

$$I(V) = \frac{2e}{h} \int_{\mu_1}^{\mu_2} dE T(E,V)[f(E - \mu_1) - f(E - \mu_2)] \quad (2)$$

where μ_1 and μ_2 are the chemical potentials of the electrode

1 and 2 and f is the Fermi–Dirac distribution function. Detailed descriptions of our methods can be found elsewhere.[20,22]

3. Results and Discussions

3.1. Molecular Conformation and Device Modeling. The first step of our computational study was the extraction of the optimal monolayer packing density and the corresponding molecular conformations via force-field MD simulations. We have considered both the self-assembled monolayer (SAM)[16] and Langmuir monolayer (LM)[23] cases and found similar optimal packing densities and molecular conformations. For the present investigation, we incorporated the SAM with the molecular structure **R1** [Figure 1b] as the starting point of the device model construction. First, we briefly outline the procedure and results of MD simulations for rotaxane SAMs. We constructed models at varying SAM packing densities by using $m \times n$ ($m, n = 3 - 7$) Au(111) supercell slabs as the template. While fixing the electrode atoms, we first conducted canonical ensemble (NVT) MD simulations at 300 K for 100 ps with 1-fs time steps to pre-equilibrate the system using the fully extended structure as the initial condition [Figure 2a]. We constructed superstructures made of 4 × 4 = 16 rotaxanes, and we performed another 3-ns NVT MD simulations (1 ns for equilibration and 2 ns for collecting statistics). We identified the 4 × 4 Au(111) grid/molecule or the area of 115 Å²/molecule as the most stable [2]rotaxane monolayer packing density, which is in good agreement with the experimental values of ~119– 134 Å²/molecule for different types of rotaxanes.[5]

Structures of the molecule that relaxed within the monolayer with the height of 34.1 Å [Figure 2b] are far from the ideal
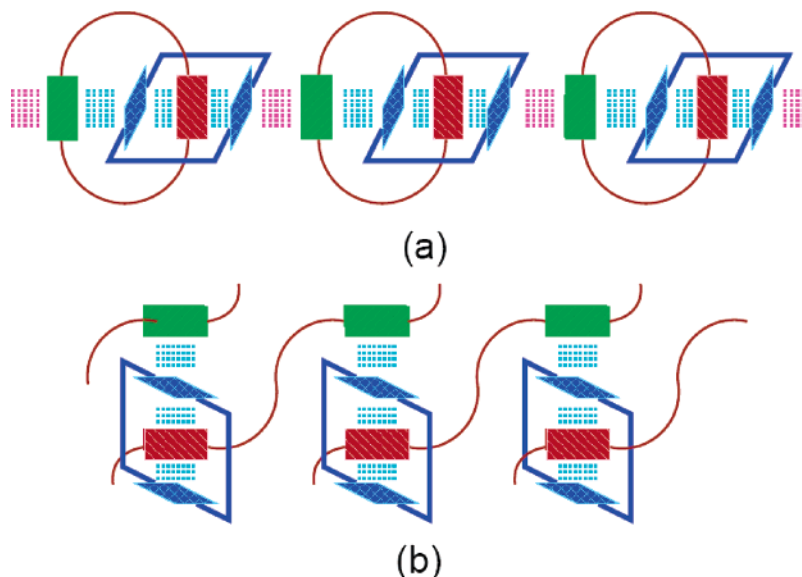
Figure 3. Schematics of spatial distribution of redox-active components, TTF (green forward diagonal hatched), DNP (red backward diagonal hatched), and CBPQT[4+] (blue cross hatched) within the (a) catenane and (b) rotaxane monolayers in their MSCC configurations.

extended rod shape with the length of 65.5 Å [Figure 2a]. Important aspects of the molecular structures for the device performance, which will be a major point of consideration throughout this paper, are as follows: We first note that dimensional changes between GSCC and MSCC in the rotaxane device are minimal. This indicates that the structural transformation between the two conformations would be possible within the solid-state device setting where the molecules are confined between electrodes. Next, the arrangement of catenane and rotaxane monolayers, schematically sketched in Figure 3, indicates that the redox-active components are arranged in parallel within the catenane monolayer and in serial within the rotaxane monolayer. Importantly, electrons can flow along the π-orbital backbones of the redox-active elements in the catenane case, while they have to tunnel approximately perpendicularly through the stacked $\pi-\pi$ planes in the rotaxane case.

In constructing GSCC and MSCC device models for the successive quantum mechanical calculations, the focus was simplifying the molecular structure to reduce the computational cost while retaining the essential features of the full molecular structure. For the GSCC configuration, we used the molecules **R1** in GSCC relaxed at the optimal monolayer packing density, 4×4 Au(111) grid/molecule, as the starting point of device modeling [Figure 2b]. We simplified the molecular structure **R1** to the structure **R2** by removing stoppers and replacing the end oxygen atoms of the two ether linkages by sulfur atoms [Figure 1c]. We here assumed that stoppers only act as a means to provide enough area for the mechanical switching of individual molecules[5] and do not affect the electrical transport properties. However, we will show in section 3.3 that this is not such an obvious conclusion. Next, we thiol-bridged the simplified molecule to the Au(111) electrodes with the electrode—electrode gap distance of 28 Å. As we do not explicitly include the rotaxane's bulky stoppers as well as the native oxide layer in our models, we instead planted four propylthiolate (CH$_3$—CH$_2$—CH$_2$—S, C3T) molecules between the molecular core region and each of the bottom and top metal electrodes as the insulating layer [Figure 2c]. We performed another 200 ps of MD simulations [Figure 2d]. Finally, we removed C3Ts and simplified the **R2** structure to the **R3** structure by replacing the end of the first ether linkages by methyl (CH$_3$) groups [Figure 1d]. By placing it between the electrodes with the 22-Å
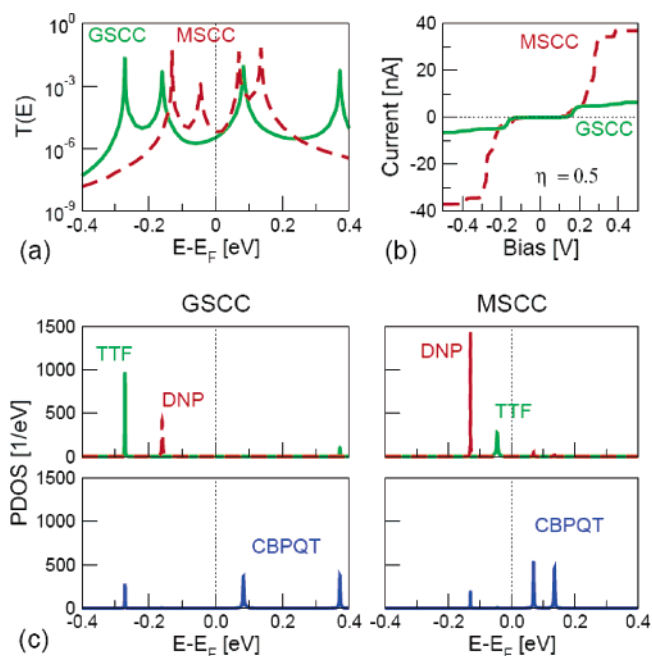
Figure 4. (a) Transmissions of a rotaxane device in GSCC (solid green lines) and MSCC (dashed red lines) and (b) their $I-V$ characteristics. (c) Corresponding TTF (solid green lines), DNP (dashed red lines), and CBPQT[4+] (dot-dashed blue lines) PDOS within GSCC and MSCC.

electrode—electrode gap distance, we finalized the device model by allowing only the two CH$_3$ ends to relax [Figure 2e]. A similar procedure was repeated to prepare corresponding MSCC device models [Figure 2f].

3.2. Device Charge Transport Characteristics: Efficiency of $\pi-\pi$ Tunneling. The transmission, $I-V$ characteristics, and projected density of states (PDOS) of our device model in its representative GSCC and MSCC configurations are shown in Figure 4. We should emphasize that, while in the experiments[3–5] molecules were insulated from the poly-Si bottom electrode and the Ti—Al top electrode by a SiO$_2$ layer and stoppers, respectively, we did not include the rotaxane's bulky stoppers as well as the native oxide layer in our models. So, in calculating the $I-V$ characteristics via eq 2 we assumed $T(E,V) = T(E,0)$ and that the redox-active components are symmetrically placed between the electrodes[5] by setting $\mu_1 = E_F - \eta$ eV and $\mu_2 =$

Efficiency of $\pi-\pi$ Tunneling

J. Phys. Chem. C, Vol. 111, No. 12, 2007 **4835**
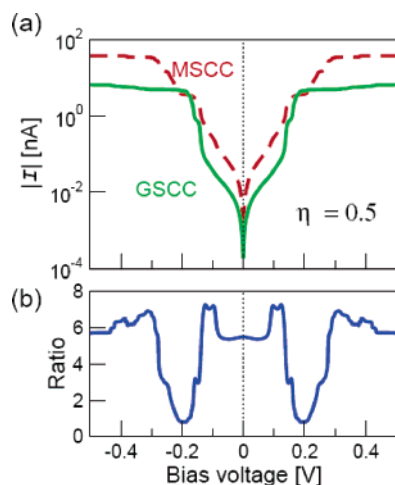
Figure 5. (a) The average $I-V$ characteristics in GSCC (solid green line) and MSCC (dashed red line) rotaxane devices and (b) the resulting switching ratio with $\eta = 0.5$.

$E_F + (1-\eta)$ eV.[24] We first point out important aspects of the device characteristics as follows:

(i) The conduction channels near E_F are dominated by four resonant transmission peaks in both configurations. HOMO and HOMO-1 transmission peaks are located closer to E_F (by $\sim$0.12 eV in this case) in MSCC than in GSCC. While the position of LUMO is similar in GSCC and MSCC, the position of LUMO+1 level is much higher (by $\sim$0.24 eV in this case) in GSCC than in MSCC [Figure 4a].

(ii) The smaller HOMO−LUMO gap and the larger transmission at E_F in MSCC than in GSCC result in a larger current in MSCC (ON) than in GSCC (OFF) when the device is probed using a small bias voltage [Figure 4b].

(iii) Characterizing the transmission peaks via PDOS [Figure 4c], we find that the transmission peaks correspond to the frontier orbitals of the redox-active elements: In GSCC, HOMO from DNP and HOMO-1 from TTF, and LUMO and LUMO+1 from CBPQT[4+]. In MSCC, HOMO is from TTF and HOMO-1 is from DNP.

These charge transport characteristics of the rotaxane device model are quite similar to those of the previously considered catenane counterparts.[13,14] We have thus demonstrated that the device switching mechanism based on the coherent charge tunneling universally applies to the rotaxane and catenane families irrespective of significant difference in the arrangement of redox-active components in the two molecules. As pointed out previously, this then confirms the high efficiency of the electron tunneling through the $\pi-\pi$ stacking in the rotaxane device. The efficiency of $\pi-\pi$ tunneling is particularly evident from the strongly resonant transmission peaks.

To further test the relevance of this conclusion, we monitored the fluctuation of the transmission peaks within GSCC and MSCC through several MD snapshots [Figure 2d]. For the reliability, two independent MD runs were carried out. Then, by selecting four random configurations with the 10-ps time interval from each run, we prepared eight molecular geometries for each GSCC and MSCC case. As shown in Figure 5, the average $I-V$ data show a clear ON/OFF switching behavior with the switching ratio of about 5, which is in good agreement with experiments.[5]

Having confirmed the universality of the device switching mechanism based on the energetic movement of frontier orbitals accompanying conformational switching, we now focus on the specific properties of the rotaxane device compared with those of the catenane counterpart.[13,14] The first difference we observe is the rather nonuniform transmission peak heights in the rotaxane device: the CBPQT[4+]-complexed backbone units (TTF in GSCC and DNP in MSCC) show better conductance than the uncomplexed elements (DNP in GSCC and TTF in MSCC). This feature is different from that of the catenane device, for which the similar location and arrangement of TTF, DNP, and CBPQT[4+] with respect to electrode surfaces resulted in more or less equivalent transmission peak heights. The second and more important difference is that the GSCC HOMO and HOMO-1 levels are, respectively, originated from DNP and TTF in the present rotaxane device model. On the other hand, for the GSCC catenane case, we found that the HOMO and HOMO-1 levels have TTF and DNP origins, respectively. The energetic order of TTF and DNP levels assumes critical importance for the activation of mechanical switching, and in section 3.3 we will consider the accuracy of this level assignment and its implication.

3.3. Energetic Order of TTF and DNP Levels: Importance of Molecule−Metal Interface. We have so far discussed the electrical switching of the rotaxane molecular junctions, which was experimentally observed via a small "read" bias ($-0.2 \sim +0.2$ V). It should be emphasized that the critical precondition of observing this *electrical* switching is the reversible *mechanical* switching of the molecules between GSCC and MSCC that were experimentally induced by applying a large "write" bias ($\sim\pm2$ V) within the tunnel junctions: Upon applying a high bias voltage to the molecules in GSCC, TTF is oxidized to its dication (TTF[2+]).[3] Then, the Coulomb repulsion between TTF[2+] and CBPQT[4+] causes the CBPQT[4+] ring to move to the DNP site, or transforms the rotaxane molecules to their MSCC configurations. Only after this conformational switching, observation of electrical switching is possible.

In this "conformational switching at high bias voltages → electrical switching at low bias voltages" scenario, the energetic position of TTF in GSCC being HOMO is crucial, so that TTF (rather than DNP) can be oxidized and the conformational switching to MSCC induced. As described in section 3.2, however, we found that HOMO has the DNP (rather than TTF) origin within our calculations. This is the major difference between the present rotaxane device model and previous catenane device models.[13,14] We found a similar assignment in the five out of the total eight GSCC models that were used to obtain the average $I-V$ curve shown in Figure 5. This is in contrast to our finding for the catenane device case, where all the models we considered had TTF-originated HOMO.[14] If this difference is a general behavior, then, because about half of the rotaxane molecules will not switch, it implies that the rotaxane is a poor device candidate compared with the catenane counterpart. We now show that the above DNP-originated HOMO in some rotaxane device models is due to our simplification of device models, particularly the interface between molecules and electrodes, rather than intrinsic properties of rotaxanes.

We note that the **R3** device model [Figure 2e] was generated from the MD simulations of the **R2** model with the C3Ts, instead of the stoppers in the original **R1**, separating the molecular core from the electrodes. To check the effect of this model simplification, we calculated the transmissions of the original **R2** GSCC model [Figure 2d] with and without C3Ts. The transmission data and the corresponding TTF and DNP PDOS curves are shown in Figure 6. The transmission of the simplified **R3** GSCC model [Figure 4a] is also reproduced in Figure 6a. Note that we have the same configurations of molecular cores in all these models. First, we observe that the
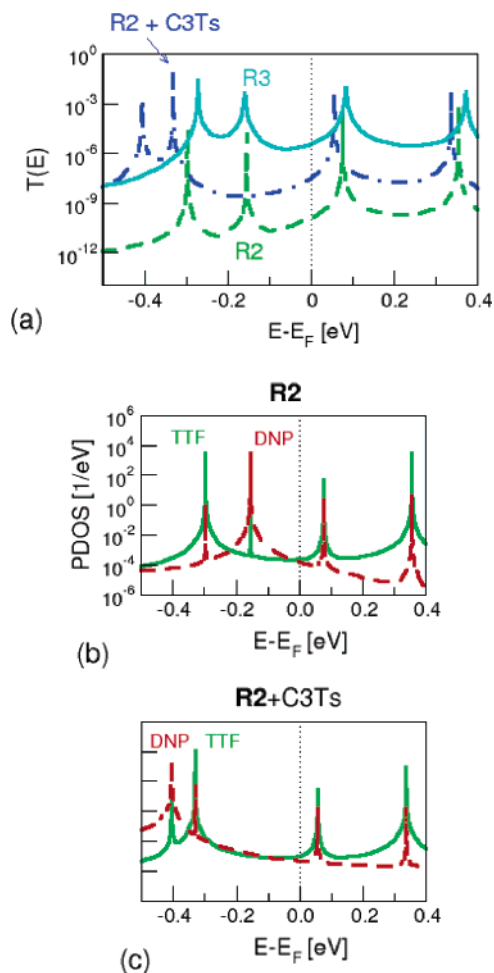
Figure 6. (a) Transmissions of the GSCC devices based on the rotaxane **R3** [reproduced from Figure 4a] model and **R2** models with and without C3Ts. TTF (solid green lines) and DNP (dashed red lines) PDOS of the (b) **R2** model without C3Ts and (c) **R2** model including C3Ts. Note that the order of TTF and DNP is different.

R2 GSCC model *without* C3Ts shows a significantly reduced transmission (by a factor of $\sim 10^{-5}$ near E_F) compared with that of the **R3** case. This is a natural consequence of the extra vacuum gaps (total of ~ 6 Å) introduced between the molecular core and the Au(111) electrode surfaces. However, the level positions of frontier oribitals are essentially identical to those of the **R3** GSCC model. Also, the origin of HOMO and HOMO-1 is respectively DNP and TTF [Figure 6b], which is identical to that of the GSCC **R3** model [Figure 4c].

On the other hand, the transmission and PDOS of the **R2** GSCC model *with* C3Ts are noticeably different from those of the **R3** GSCC model, or we observe that the role of C3Ts is rather critical: The transmission amplitude increases by factor of $\sim 10^3$ near E_F. The position of HOMO and HOMO-1 are shifted downward by about 0.2 eV. Most importantly, the order of HOMO and HOMO-1 character is reversed from DNP−TTF to TTF−DNP [Figure 6c]. As emphasized earlier, the energetic ordering of the two HOMOs being TTF−DNP is exactly what is required to induce a mechanical switching.

This comparison shows that, although the simplification of **R2** to **R3** itself does not fundamentally change the character of the system, the direct contact of the molecular core with the metal electrode surface results in an important qualitative modification. Reminding that the main objective of our device modeling (summarized in Figure 2) was to simplify the system as much as possible while preserving its essential character, the

reversal of TTF and DNP levels, a rather important qualitative failure, implies that our device models are rather incomplete. For a definitive and quantitative analysis of the rotaxane device, we thus plan to incorporate a full molecular structure including stoppers in the future.

4. Conclusions

In this article, devising [2]rotaxane device models that incorporate realistic molecular monolayer conformations at an optimal packing density but are still simple enough for quantum mechanical calculations, we investigated the coherent electron tunneling properties of rotaxane devices. By comparing the rotaxane devices with their catenane counterparts, we particularly considered the effects of energetic and spatial distributions of redox-active components on the device switching mechanism. First, focusing on the coherent charge transport through the core of rotaxane molecules, we observed an electrical switching behavior similar to that in the catenane device. We thus demonstrated (i) the efficiency of electron tunneling through the $\pi-\pi$ stacked redox-active components within the rotaxane SAMs and (ii) the universality of the switching mechanism based on the energetic movement of HOMOs. Second, however, we found in some GSCC configurations the order of HOMO and HOMO-1 is DNP−TTF rather than TTF−DNP. With the former energetic alignment, the molecule cannot be induced to conformationally switch from GSCC to MSCC, so the electrical switching (at least based on the mechanism we proposed) cannot be observed. We traced the origin of this behavior to our simplification of device models, which resulted in the direct contact of redox-active components with the metal electrode surfaces. We therefore concluded that incorporating device models based on the full molecular structure including stoppers is necessary for a definitive and quantitative conclusion. While we leave this for future work, we thus demonstrated that the molecule-metal contacts are an important element in designing molecular electronic devices.

References and Notes

(1) Stoddart, J. F.; Tseng, H.-R. *Proc. Nat. Acad. Sci. U.S.A.* **2002**, *99*, 4797.

(2) Collier, C. P.; Wong, E. W.; Belohradský, M.; Raymo, F. M.; Stoddart, J. F.; Kuekes, P. J.; Williams, R. S.; Heath, J. R. *Science* **1999**, *285*, 391.

(3) Collier, C. P.; Mattersteig, G.; Wong, E. W.; Luo, Y.; Beverly, K.; Sampaio, J.; Raymo, F.; Stoddart, J. F.; Heath, J. R. *Science* **2000**, *289*, 1172.

(4) Collier, C. P.; Jeppesen, J. O.; Perkins, J.; Wong, E. W.; Heath, J. R.; Stoddart, J. F. *J. Am. Chem. Soc.* **2001**, *123*, 12632.

(5) Luo, Y.; Collier, C. P.; Jeppesen, J. O.; Nielsen, K. A.; Delonno, E.; Ho, G.; Perkins, J.; Tseng, H.-R.; Yamamoto, T.; Stoddart, J. F.; Heath, J. R. *Chem. Phys. Chem.* **2002**, *3*, 519.

(6) Service, R. F. *Science* **2003**, *302*, 556.

(7) Heath, J. R.; Stoddart, J. F.; Williams, R. S. *Science* **2004**, *303*, 1136.

Efficiency of π−π Tunneling

J. Phys. Chem. C, Vol. 111, No. 12, 2007 **4837**

(8) Chen, Y.; Ohlberg, D. A. A.; Li, X.; Stewart, D. R.; Williams, R. S.; Jeppesen, J. O.; Nielsen, K. A.; Stoddart, J. F.; Olynick, D. L.; Andersen, E. *Appl. Phys. Lett.* **2003**, *82*, 1610.

(9) Stewart, D. R.; Ohlberg, D. A. A.; Beck, P. A.; Chen, Y.; Williams, R. S.; Jeppesen, J. O.; Nielsen, K. A.; Stoddart, J. F. *Nano Lett.* **2003**, *4*, 133.

(10) Lau, C. N.; Stewart, D. R.; Williams, R. S.; Bockrath, M. *Nano Lett.* **2004**, *4*, 569.

(11) Diehl, M. R.; Steuerman, D. W.; Tseng, H.-R.; Vignon, S. A.; Star, A.; Celestre, P. C.; Stoddart, J. F.; Heath, J. R. *Chem. Phys. Chem.* **2003**, *4*, 1335.

(12) Deng, W.-Q.; Muller, R. P.; Goddard, W. A., III. *J. Am. Chem. Soc.* **2004**, *126*, 13562.

(13) Kim, Y.-H.; Jang, S. S.; Jang, Y. H.; Goddard, W. A., III. *Phys. Rev. Lett.* **2005**, *94*, 156801.

(14) Kim, Y.-H.; Jang, S. S.; Goddard, W. A., III. *Appl. Rev. Lett.* **2006**, *88*, 16312.

(15) Mayo, S. L.; Olafson, B. D.; Goddard, W. A., III. *J. Phys. Chem.* **1990**, *94*, 8897.

(16) Jang, S. S.; Jang, Y. H.; Kim, Y.-H.; Goddard, W. A., III; Flood, A. H.; Laursen, B. W.; Tseng, H.-R.; Stoddart, J. F.; Jeppesen, J. O.; Choi, J. W.; Steuerman, D. W.; DeIonno, E.; Heath, J. R. *J. Am. Chem. Soc.* **2005**, *127*, 1563.

(17) Rappé, A. K.; Goddard, W. A., III. *J. Phys. Chem.* **1991**, *95*, 3358.

(18) Fuchs, M.; Scheffler, M. *Comput. Phys. Commun.* **1999**, *119*, 67.

(19) Perdew, J. P.; Burke, K.; Ernzerhof, M. *Phys. Rev. Lett.* **1996**, *77*, 3865.

(20) Kim, Y.-H.; Tahir-Kheli, J.; Schultz, P. A.; Goddard, W. A., III. *Phys. Rev. B* **2006**, *73*, 235419.

(21) Datta, S. *Quantum Transport: Atom to Transistor*; Cambridge University Press: Cambridge, U.K., 2005.

(22) Kim, Y.-H.; Jang, S. S.; Goddard, W. A., III. *J. Chem. Phys.* **2005**, *122*, 244703.

(23) Jang, S. S.; Jang, Y. H.; Kim, Y.-H.; Goddard, W. A., III; Choi, J. W.; Heath, J. R.; Laursen, B. W.; Flood, A. H.; Stoddart, J. F. *J. Am. Chem. Soc.* **2005**, *127*, 14804.

(24) Datta, S.; Tian, W.; Hong, S.; Reifenberger, R.; Henderson, J. I.; Kubiak, C. P. *Phys. Rev. Lett.* **1997**, *79*, 2530.